B. Electron Motion in Highly Excited States and Radiationless Transitions. General Dynamical Theory and Experiment

Intramolecular Dynamics and Charge Separation in Large Systems

Joshua Jortner and M. Bixon

School of Chemistry, Tel-Aviv University, Tel-Aviv, Israel

Key Words: Effective Hamiltonian / Electron Transfer / Molecular Structure / Radiationless Transitions / Rydberg Excitation / ZEKE Rydbergs

We adopt the theory of intramolecular dynamics to explore charge separation and recombination in two classes of 'isolated' solvent-free molecular systems: (A) Supermolecules containing bridged electron donor and electron acceptor, where electron transfer occurs on a spatial scale of ~ 10 Å. (B) Ultrahigh molecular Rydberg excitations with a principle quantum number $n \simeq 50-300$ and spatial dimensions of ~ 10^4 Å, where relaxation processes, e.g., electron-core recombination via internal conversion or predissociation, and charge separation by autoionization, are manifested. The molecular limit for photoinduced long-range ET in isolated supermolecules [class (A)] is treated on the basis of the statistical limit for interstate radiationless transitions, which involve either a direct or a mode-selective mediated coupling. The level structure, optical excitation modes and dynamics of high molecular Rydbergs [class (B)] interrogated by time-resolved ZEKE (zero-electron kinetic energy) spectroscopy, are treated by the effective Hamiltonian formalism. We pursue the formal analogy between the coupling, accessibility and decay of ultrahigh Rydbergs in an external weak ($F = 0.01-1.0$ V/cm) electric field and intramolecular (interstate and intrastate) relaxation in a bound level structure. Model calculations for the field-induced (l) mixing reveal that the Rydberg dynamics is characterized by two distinct (~ ns and ~ μs) time scales. Up to date, long time-resolved (10 μs – 100 ns time scales) nonexponential decay of ZEKE Rydbergs was experimentally documented, in accord with our analysis. The predicted existence of the short decay times (1 – 10 ns) was not yet subjected to an experimental test.

I. Prologue

We shall be concerned with the dynamics of charge separation and recombination in two classes of 'isolated' solvent-free molecular systems:

(A) Supermolecules containing an electron donor (D)-acceptor (A) pair separated by a molecular bridge [1 – 5]. In contrast to conventional wisdom [6 – 9], photoinduced electron transfer (ET) can occur in isolated supermolecules [10 – 17]. These systems, which are of considerable interest in chemistry, molecular electronics (e.g., molecular switches) and biophysics (in the context of artificial photosynthesis [18]) are characterized by spatial dimensions of 10 – 100 Å.

(B) Ultrahigh Rydberg excitations of molecules. Such one-electron excitations, which are characterized by large principal quantum numbers $n \simeq 50-300$, have spatial dimensions of ~ 10^4 Å. Such microstructures are of considerable interest in the context of novel relaxation processes [19 – 22], e.g., Rydberg-electron-core recombination [22], charge separation by autoionization [19 – 22], and chemical reactivity [23].

The conceptual framework for the understanding of charge separation and relaxation in these two classes of large systems rests on intramolecular dynamics, i.e., radiationless transitions, in isolated large molecules [24 – 34]. The evolution of the conceptual basis for radiationless transitions originated from the related, but distinct field of dynamics in condensed phase, which was pioneered by Huang and Rhys [35], Kubo [36], Lax [37], and Kubo and Toyozawa [38] in the context of the theory of electron-hole recombination in semiconductors. Conceptually and physically isomorphous classes of radiationless phenomena pertain to the theoretical foundations of electron transfer processes in solution, whose exploration was pioneered by Marcus [6, 7], and energy transfer processes, which were elucidated by Förster [39]. When this significant progress was accomplished in the 1950's, no one realized the interrelationship between condensed-matter relaxation, e.g., electron-hole recombination, electron transfer and energy transfer, and intramolecular relaxation, e.g., intersystem crossing and internal conversion in large molecules. At that time some experimental information was already available on intramolecular relaxation in large molecules embedded in a condensed medium, i.e., a solution or a glass. Kasha formulated his rules to characterize internal conversion and intersystem crossing of solvated organic molecules [40], while Beer and Longuet-Higgins provided striking experimental evidence for the internal conversion of the first singlet excited state of azulene in solution [41]. Guided by the experimental background, the first theories of relaxation of large molecules focused on the coupling to the medium as an essential ingredient inducing electronic-vibrational conversion. Robinson and Frosch [42] proposed sequential interstate electronic coupling and medium-induced vibrational relaxation, Gouterman [43] alluded to medium phonon emission, while Lin [44] and Lin and Bersohn [45] considered medium and intramolecular multiphonon processes. A central ingredient of electronic relaxation in large molecules originated from the seminal experiments of

  0005-9021/95/0303-0296 $ 10.00+.25/0

Kistiakowski and Parmenter, which demonstrated the occurrence of intersystem crossing in the 'isolated' collision-free benzene molecule [46]. The iconoclastic implications of the occurrence of irreversible relaxation in a bound level structure were fully realized by Kistiakowski and Parmenter, who stated that their results may be incompatible with the laws of quantum mechanics [46]. The intramolecular nature of radiationless transitions in a bound level structure was established by our theoretical model [24–28], which rests on near-resonance coupling, the dynamics of wavepackets of mixed bound states, finite time evolution, and practical irreversibility in a dense bound level structure of a vibrational quasicontinuum. This general conceptual framework is applicable both for interstate coupling [24–28, 30–34], which involves two electronic configurations coupled by nuclear momenta (i.e., the breakdown of Born-Oppenheimer separability), or/and spin-orbit interaction, as well as for intrastate coupling, which involves a single electronic configuration with rotational-vibrational states coupled by anharmonic or coriolis interactions [33, 34]. This theoretical framework is of wide applicability for the study of elementary photoinduced chemical processes, i.e., charge separation between localized states in isolated molecules (class A) and novel intramolecular relaxation in molecular microsystems (class B).

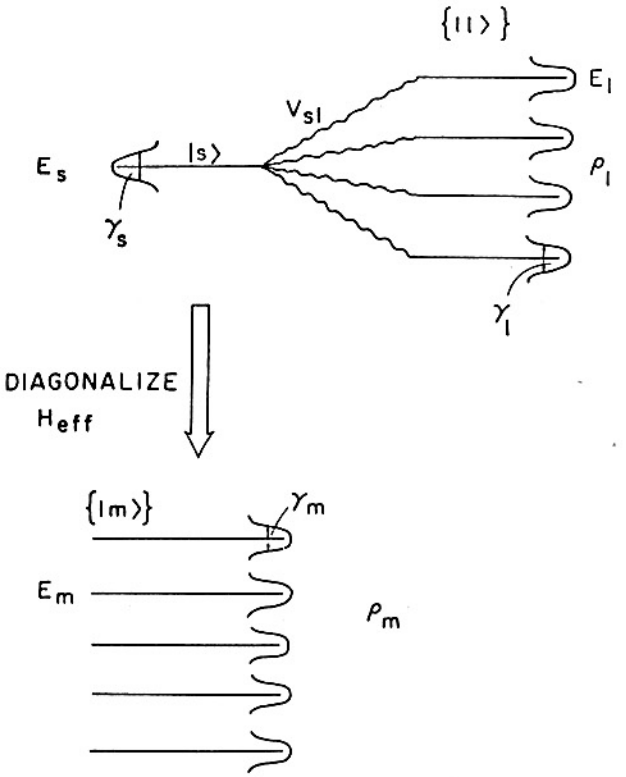

Fig. 1
The application of the effective Hamiltonian formalism for interstate and intrastate intramolecular coupling and dynamics. The zero-order states $|s\rangle$ and $\{|l\rangle\}$ are characterized by the energies E_s and $\{E_l\}$, respectively, and by the decay widths γ_s and $\{\gamma_l\}$. V_{sl} represents the intramolecular (interstate or intrastate) coupling between the doorway state $|s\rangle$ and the $\{|l\rangle\}$ manifold, which is characterized by the density of states ρ_l. Diagonalization of the effective Hamiltonian results in a set of independently decaying levels $\{|m\rangle\}$, i.e., generalized molecular eigenstates, characterized by energies $\{E_m\}$, decay widths $\{\gamma_m\}$, and density of states ρ_m

II. Intramolecular Dynamics

The central ingredients of the theory of intramolecular dynamics [24–34] in a bound level structure are:

(1) The characterization of the level structure. This requires the characterization of the appropriate zero-order states and their (small) couplings.
(2) The accessibility of the zero-order states, leading to the specification of the doorway state(s) of the system.
(3) The decay channels of the zero-order states, specifying their decay to genuine (radiative decay, predissociation, autoionization) continuum channels, which are characterized by appropriate decay widths.
(4) The excitation initial conditions, which are governed by the (optical) excitation modes.

Ingredients (1) and (3) allow for the construction of the (complex) independently decaying molecular levels $\{|m\rangle\}$, which are obtained from the diagonalization of the effective Hamiltonian [29–32, 34]

$$\mathbf{H}_{\text{eff}} = \mathbf{H}_{\text{M}} - (\text{i}/2)\boldsymbol{\Gamma} \ , \tag{1}$$

where $\mathbf{H}_{\text{M}}$ is the molecular Hamiltonian and $\boldsymbol{\Gamma}$ is the decay matrix (Fig. 1). The $\{|m\rangle\}$ states are characterized by the complex energies

$$\varepsilon_m = E_m - \frac{\text{i}}{2}\gamma_m \ , \tag{2}$$

where $\{E_m\}$ are the energy levels, while $\{\gamma_m\}$ represent the decay widths. Relevant time-resolved observables for broad-band excitation, which are based on ingredients (2) and (4), involve the population probability of the doorway state

$$P^{(\text{D})}(t) = \left| \sum_m \left| A_m \right|^2 \exp\left(\frac{-\text{i}E_m t}{\hbar} - \frac{\gamma_m t}{2\hbar} \right) \right|^2 , \tag{3}$$

where $A_m = \langle g|\hat{\mu}|m\rangle$ are the excitation amplitudes of the $\{|m\rangle\}$ manifold, and the energy-resolved (radiative) decay probability to a vibrational level $|g v\rangle$ of the ground electronic state

$$P^{(\text{v})}(t) = \left| \sum_m A_m B_m^{\text{v}} \exp\left(\frac{-\text{i}E_m t}{\hbar} - \frac{\gamma_m t}{\hbar} \right) \right|^2 , \tag{4}$$

where $B_m^{\text{v}} = \langle m|\hat{\mu}|g v\rangle$ are the transition amplitudes. These probabilities constitute Fourier sums damped by real decay exponents, they may involve either superposition of exponentials (for a sparse level structure) or an exponential decay of a giant resonance (in the statistical limit), and may result in quantum beats (in the intermediate level structure).

The character and dynamical manifestations of the sparse, intermediate and statistical level structures [27, 28, 30–32, 34] (Fig. 2) can be inferred in a transparent way from the lineshapes $L(E) = -\mathrm{Im}\, G(E)$, where the Green's function is $G(E) = (E - H_{\mathrm{eff}})^{-1}$. The classification of the level structures (Fig. 2) is specified by the coarse grained (interstate or intrastate) coupling V, the density of states of the proper symmetry ρ, and the decay widths γ. The limit of isolated states (case 1), with $V\rho < 1$, constitutes the spectroscopist's paradise, when distinct 'pure' rotational-vibrational levels can be observed. For the strongly coupled situation, with $V\rho > 1$, the sparse ($\gamma\rho < 1$), the intermediate ($\gamma\rho \sim 1$) and the statistical ($\gamma\rho \gg 1$) level structures (Fig. 2) can be realized.

III. The Statistical Limit and Mode Selectivity

The statistical limit corresponds to the extreme situation of overlapping resonances, where the whole structure in the spectrum is washed out (Fig. 2). The absorption lineshape is Lorentzian (width Γ_l), with the lifetime of the doorway state being $\tau = \hbar/\Delta_l$. The experimental observations of a Lorentzian absorption lineshape of the electronic origins (which precludes IVR) of some large molecules, e.g., the S_1 origin of azulene ($\tau \simeq 800 \pm 200$ fs) [47], the S_2 origins of phenanthrene ($\tau = 470$ fs) [48], and of free-base porphyrin ($\tau \simeq 450$ fs) [49], constitutes the victory of dynamics over spectroscopy for a highly congested level structure.

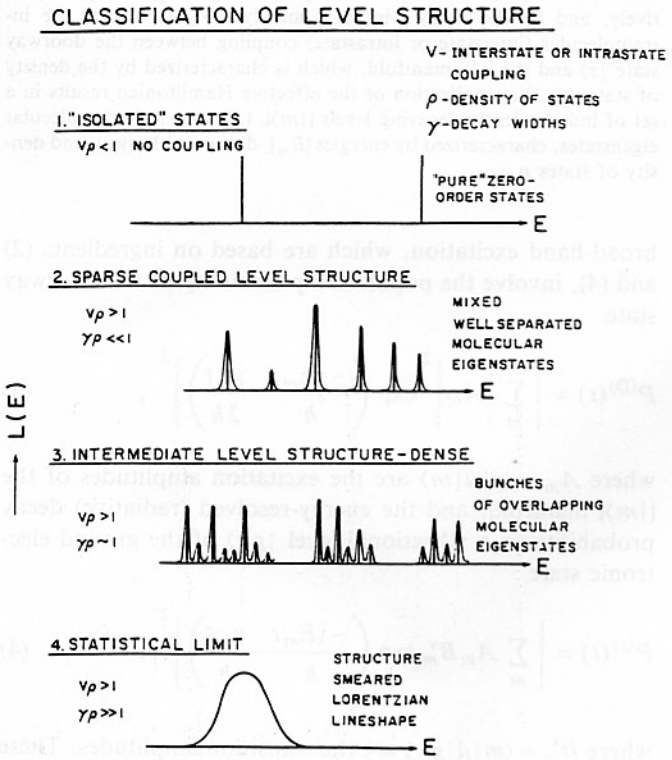

Fig. 2
Classification of intramolecular level structure. The relevant energetic and dynamic parameters are: the (interstate or intrastate) coupling V, the density of the independently decaying levels ρ and their decay widths γ. The spectra exhibit the energy-dependent lineshape $L(E)$ vs. E

However, the characteristics of interstate coupling and intramolecular relaxation can be more complex and interesting due to resonance effects [50]. Mediated intersystem crossing [24] from a S_1 vibronic state to the dense lowest triplet $\{T_1\}$ manifold can be induced by the sequential coupling via a sparse manifold $\{T_x\}$ of vibronic states corresponding to a higher triplet state. The theory of mediated coupling and relaxation predicts the occurrence of resonances originating from $\{T_x\}$-$\{T_1\}$ vibronic coupling, which mediate the decay of the S_1 doorway state [50]. When the level structure of the $\{T_x\}$-$\{T_1\}$ resonances is sparse, the decay rate is very sensitive to the energy gaps between the S_1 and the T_x states. Accordingly, climbing up the vibrational levels in the S_1 manifold above its electronic origin will result in a wide variation of their radiationless decay rates, exhibiting a marked mode selectivity of mediated intersystem crossing. Such dramatic vibrational mode-selective effects are revealed in the absolute fluorescence quantum yields from photoselected vibronic levels in the S_1 manifold of 9,10-dibromoanthracene DBA [50] (Fig. 3), where the irregular variance of the nonradiative lifetimes spans about three orders of magnitude. These resonance effects for the decay of the S_1 state of DBA span the excess vibrational energy range $E_v = 0 - 800\ \mathrm{cm}^{-1}$ above the electronic origin of the S_1 electronic manifold, while at higher E_v mode selectivity is eroded due to intramolecular vibrational energy redistribution.

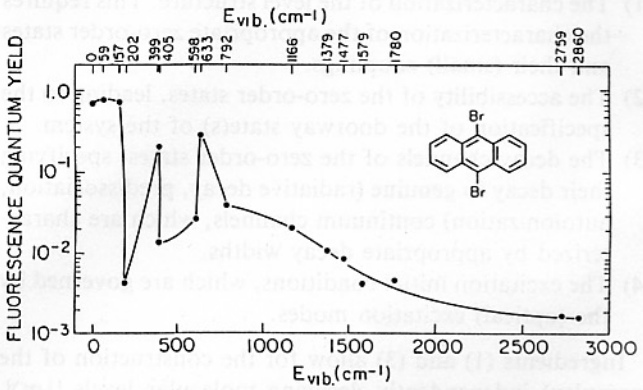

Fig. 3
Absolute fluorescence quantum yield from photoselected vibronic levels of the S_1 manifold of jet-cooled 9,10-dibromoanthracene (Amirav, Horowitz, and Jortner, Ref. [50]). The numbers of the upper horizontal scale represent the energies of the vibronic levels above the electronic origin of S_1. Note the resonance effects in the energy range $E_{\mathrm{vib}} = 0 - 800\ \mathrm{cm}^{-1}$ exhibiting the variation of the nonradiative decay width over the numerical range of 300, which manifest mode selectivity. IVR within the S_1 manifold sets in at $\gtrsim 800\ \mathrm{cm}^{-1}$ eroding mode selectivity at higher energies

The theory of intramolecular radiationless transitions in the statistical limit provides a predictive quantitative framework for ubiquitous processes in photochemistry. In this context photochemistry, and in particular photoinduced ET, in large, isolated supermolecules is of con-

siderable interest. We have recently advanced [10 – 12] the molecular limit for long-range ET in solvent-free supermolecules, which will now be addressed.

IV. Long-Range ET in Isolated Supermolecules

ET reactions in chemistry, physics and biology have been almost exclusively explored in D – A systems embedded in a medium, e.g., a polar solvent, a nonpolar molecular solvent, a glass or a protein [8, 9, 18]. From the point of view of general methodology, such ET processes correspond to a broad class of nonradiative electronic processes in condensed medium, which involve the conversion of electronic to vibrational energy [24 – 34]. Nonradiative ET can be realized as an intramolecular transition in a solvent-free isolated supermolecule. Recent theoretical [10 – 12, 16] and experimental [13 – 15, 17] studies have challenged the conventional wisdom regarding the dominating role of the medium coupling in ET. We have recently proposed [10 – 12] that long-range ET can occur in isolated, solvent-free supermolecules and have analysed the structural constraints for the occurrence of this intramolecular radiationless transition. On the experimental front [13 – 15], in a single case conclusive experimental evidence has been reported by Verhoeven et al. for photoinduced long-range ET in the isolated, jet-cooled 1-phenyl-4-((4-cyano-1-naphthyl)methyl)piperidine semirigid supermolecule and some of its derivatives under solvent-free conditions.

We consider long-range ET in a structurally rigid, solvent-free DBA supermolecule (where B represents a molecular bridge). Intramolecular ET will be realized when an 'initially excited' vibronic state of (DBA)* is quasidegenerate with a dense vibronic manifold of D^+BA^- and is effectively coupled to it [10, 12, 16], or under a somewhat more complex physical situation, when the D^+BA^- manifold mediates the relaxation of the initial DA state into another final intramolecular quasicontinuum [11].

The charge transfer state D^+BA^- constitutes the lowest spin-allowed electronic excitation, provided that sufficient electrostatic stabilization of D^+BA^- prevails, which implies a practical limit for the D – A (center-to-center) separation [10] of $R_{DA} \lesssim e^2[I(D) - E(A) - E_\infty]^{-1}$, where $I(D)$ is the donor ionization potential, $E(A)$ the acceptor electron affinity and E_∞ the electronic origin of $S_2(DBA)^*$, implying that $R_{DA} \lesssim 6-7$ Å. The order of the electronic states with increasing energy is then $S_0(DBA)$, $S_1(D^+BA^-)$ and $S_2((DBA)^*)$ (Fig. 4), where $(DBA)^*$ is a localized spin-allowed electronic excitation of DBA. Two intramolecular ET processes can be realized:

(A) Charge separation $S_2((DBA)^*) \rightarrow S_1(D^+BA^-)$ with a vibronic level of the electronically excited localized singlet state decaying into the charge transfer vibronic manifold. The initial (doorway) state of $S_2((DBA)^*)$ can be photoselectively excited by a photon $h\nu$ (Fig. 4).

(B) Charge recombination $S_1(D^+BA^-) \rightarrow S_0(DBA)$, with a vibronic level of the charge transfer state decaying into the vibrationally excited ground state manifold. The initial (doorway) state within $S_1(D^+BA^-)$ can be photoselectively excited by a photon $h\nu_{CT}$ (Fig. 4).

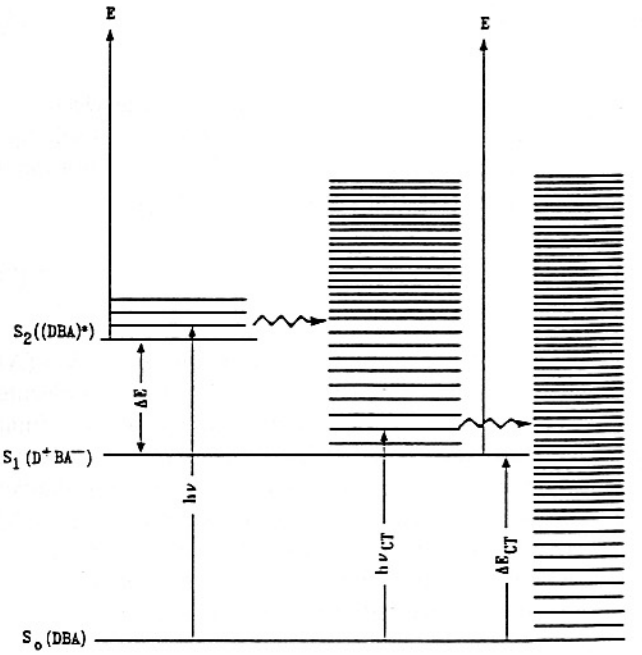

Fig. 4
Molecular level structure for ET processes in an isolated supermolecule. Optical $S_0(DBA) \xrightarrow{h\nu} S_2((DBA)^*)$ excitation selects vibronic $S_2((DBA)^*)$ level(s), which undergoes intramolecular charge separation (denoted by a horizontal arrow) to the $S_1(D^+BA^-)$ vibronic manifold. Optical $S_0(DBA) \xrightarrow{h\nu_{CT}} S_1(D^+BA^-)$ excitation selects vibronic $S_1(D^+BA^-)$ level(s), which undergo intramolecular charge recombination (denoted by a horizontal arrow) to the $S_0(DBA)$ vibronic manifold. This ladder diagram establishes the interrelationship between ET in isolated molecules and intramolecular radiationless transitions. It is gratifying that resonance Raman [53] and optical lineshapes [51] data allow for the quantification of these ladder diagrams

We can characterize the intramolecular ET processes of type (A) or (B) in terms of $|j\rangle \rightarrow \{|f\rangle\}$ effective coupling and relaxation, where the state $|j\rangle$ (with energy E_j) corresponds to a vibronic state of $S_2((DBA)^*)$ for (A) and a vibronic state of $S_1(D^+BA^-)$ for (B), while the $|f\rangle$ states (with energies E_f) correspond to the vibronic manifold of $S_1(D^+BA^-)$ for (A) and the vibronic manifold of $S_0(DBA)$ for (B). Effective interstate coupling prevails provided that the density of final states in the vicinity of E_j

$$\rho(j) = \sum_f \delta(E_j - E_f) \tag{5}$$

is sufficiently large relative to the sequential decay widths γ_j of the final states, i.e., $\gamma_j \rho_j \gg 1$, and the coupling is strong, so that $2\pi\rho(j) \sum_f |\langle j|\hat{H}|f\rangle|^2 \delta(E_j - E_f) \gg 1$, where $\hat{H}$ is the system's Hamiltonian. These conditions insure the occurrence of $|j\rangle \rightarrow \{|f\rangle\}$ relaxation in the statistical limit [24]. The intramolecular ET rate (of the initial state $|j\rangle$) in the isolated molecule is [12]

$$k_j = (2\pi/\hbar) \sum_f |\langle j|\hat{H}|f\rangle|^2 \delta(E_j - E_f) \ . \quad (6)$$

Setting $|\langle j|\hat{H}|f\rangle|^2 = V^2 F(j;f)$, where V is the electronic coupling (involving the many-electron two-center exchange integral) and $F(j;f)$ is the Franck-Condon vibrational overlap integral, the microscopic ET rates are

$$k_j = (2\pi V^2/\hbar) \sum_f F(j;f)\delta(E_j - E_f) \ . \quad (7)$$

Irreversibility of the intramolecular charge separation (A) and charge recombination (B) in the isolated supermolecule is implicitly insured by sequential decay of the final D^+BA^- manifold via radiative decay and nonradiative charge recombination in case (A) and via infrared radiative decay and possible isomerization processes within S_0(DBA) in case (B). Eq. (7) has the "Golden Rule" form for a quantum mechanical transition probability. This relation is applicable provided that interference effects between neighboring $|j\rangle$ states are negligible [16].

Invoking a coarse graining procedure, based on the assumption of the equal occupation probability for the quasidegenerate initial states within a (small) energy interval δE, the energy-dependent rate constant $k(E)$ at the initial energy E (Fig. 4) is given by [5, 10–12, 16]

$$k(E) = (2\pi V^2/\hbar)\mathrm{AFD}(E) \ . \quad (8)$$

The averaged Franck-Condon density AFD was calculated for a simple harmonic model system with two displaced nuclear potential surfaces $U_j(q)$ and $U_f(q)$, which are characterized by the same frequencies $\{\omega_1, \omega_2, \ldots, \omega_n\}$ and by the (dimensionless) displacements of the equilibrium positions of the minima of the potential surfaces $\{\Delta_1, \Delta_2, \ldots, \Delta_n\}$. The intramolecular reorganization energy is

$$\lambda = \sum_{l=1}^{n} \hbar\omega_l S_l = \sum_{l=1}^{n} \lambda_l \ , \quad (9)$$

where $S_l = \Delta_l^2/2$ is the mode-specific electron-nuclear coupling strength and $\lambda_l = \hbar\omega_l S_l$ is the mode-specific reorganization energy for a distinct vibrational mode ω_l. ΔE is the energy gap between the minima of the potential surfaces (Fig. 4). The initial and final vibronic states will be specified in terms of the occupation numbers of the vibrational modes $|j\rangle \equiv \{j_1, j_2, \ldots, j_n\}$ and $|f\rangle \equiv \{f_1, f_2, \ldots, f_n\}$, respectively. The averaged Franck-Condon density (AFD) is [5, 12]

$$\mathrm{AFD}(E) = [N(E)]^{-1}(\delta E)^{-1} \sum_{\{j\}} \sum_{\{f\}} \prod_{l=1}^{n} F(j_l;f_l)\delta_{E_j,E_f} \ . \quad (10)$$

$F(j_l;f_l)$ are the Franck-Condon factors between the initial j_l and the final f_l states of mode l.

$$F(j_l;f_l) = j!f!\exp(-\Delta^2/2) \times \left[\sum_{r=0}^{\min(j,f)} \frac{(-1)^{j+f-r}(\Delta/\sqrt{2})^{j+f-2r}}{r!(j-r)!(f-r)!}\right]^2 , \quad (11)$$

where on the RHS of Eq. (11) we abbreviate $\Delta \equiv \Delta_l$, $j \equiv j_l$ and $f \equiv f_l$. The Kronecker delta function in Eq. (10) restricts the sums over degenerate initial and final states. The normalization factors for the AFD, Eq. (10), involve the number $N(E)$ of initial vibronic states in the energy range δE around E. δE is chosen as the common divider of the vibrational frequencies and of the energy gap.

We shall present model calculations of the energy dependence of the microscopic AFD(E), which determine $k(E)$, Eq. (8), for charge recombination and for charge separation in isolated, solvent-free, jet-cooled supermolecules, where optical selection of vibronic states is not blurred by thermal sequence congestion effects and no collisional damping prevails.

(i) Charge recombination $S_1(D^+BA^-) \rightarrow S_0$(DBA) (Fig. 4). The excess vibrational energy E in the vibronic manifold of $S_1(D^+BA^-)$ (with an energy gap ΔE_{CT} relative to S_0(DBA)) is acquired by the electronic-vibrational optical excitation ($h\nu_{CT} = \Delta E_{CT} + E$) to the $S_1(D^+BA^-)$ charge transfer band. This absorption band is broad and structureless for supermolecules and DA complexes in solution [5, 51] and in isolated jet-cooled DA complexes [52], manifesting strong electron-phonon coupling.

(ii) Charge separation $S_2((DBA)^*) \rightarrow S_1(D^+BA^-)$ (Fig. 4). The excess vibrational energy E in the vibronic manifold of $S_2((DBA)^*)$ (with an energy gap ΔE relative to $S_1(D^+BA^-)$) is acquired by electronic-vibrational excitation ($h\nu = \Delta E_{CT} + \Delta E + E$) to the $S_2((DBA)^*)$ excited localized electronic state.

Our model calculations of $k(E)$ attempt to mimic the dependence of the energy-dependent ET rates on the energetic parameters, e.g., the energy gap ΔE and the intramolecular reorganization energy, $\lambda = \Sigma\lambda_l$, Eq. (9). In the choice of the input mode-specific λ_l parameters we were guided by the resonance Raman data of Markel et al. [53] for the hexamethylbenzene-tetracyano-ethylene charge transfer complex. We have subdivided the molecular modes into low frequency $\omega_1 = 200\,\mathrm{cm}^{-1}$, medium frequency $\omega_2 = 500\,\mathrm{cm}^{-1}$ and two high-frequency $\omega_3 = 1200\,\mathrm{cm}^{-1}$ and $\omega_4 = 1500\,\mathrm{cm}^{-1}$ vibrations, with the corresponding dimensionless shifts $S_1 = 6$, $S_2 = 3-1.2$, $S_3 = 1-0.4$ and $S_4 = 1-0.8$. The total intramolecular reorganization energies were taken in the range $\lambda = 5400-3400\,\mathrm{cm}^{-1}$, in accord with recent spectroscopic data for barrelene-based DBA supermolecules in hexane, which yield for the intramolecular reorganization energy $\lambda = 4600\,\mathrm{cm}^{-1}$ [51]. The energy gap for charge recombination, which is approximately corrected for solvent perturbations of the electronically excited charge transfer state, is $\Delta E_{CT} \simeq 25000-28000\,\mathrm{cm}^{-1}$ for typical barrelene-based DBA molecules

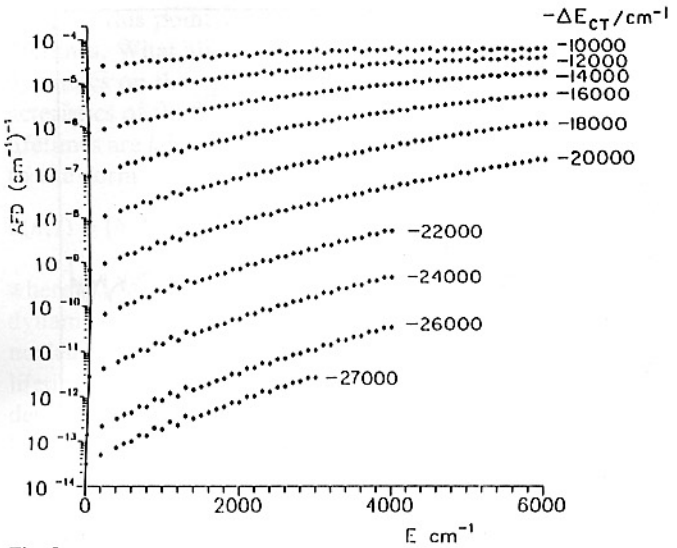

Fig. 5
Model calculations of the excess vibrational energy dependence of the average Franck-Condon density AFD(E) for intramolecular charge recombination. E is the excess energy above the zero-point energy in the $S_1(D^+BA^-)$ vibronic manifold $n = 4$, the characteristic frequencies are $\omega_1 = 200\,cm^{-1}$, $\omega_2 = 500\,cm^{-1}$, $\omega_3 = 1200\,cm^{-1}$ and $\omega_4 = 1500\,cm^{-1}$, the reduced displacements are $S_1 = 6$, $S_2 = 3$, $S_3 = 1$ and $S_4 = 1$ and $\lambda = 5400\,cm^{-1}$. The energy gaps $-\Delta E_{CT}$ in the range $12000 - 27000\,cm^{-1}$ are marked on the curves and $\delta\varepsilon = 100\,cm^{-1}$

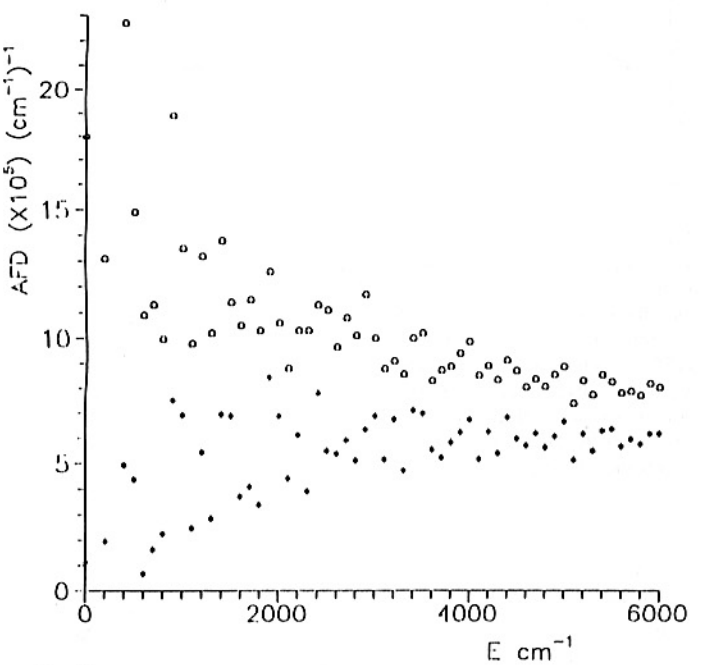

Fig. 6
Model calculations of the excess vibrational energy dependence of the average Franck-Condon density AFD(E) for intramolecular charge separation. E is the excess energy above the zero-point energy of $S_2((DBA)^*)$. $n = 4$, with the characteristic frequencies and displacements being the same as in Fig. 2. $\delta E = 100\,cm^{-1}$. (*) $-\Delta E = 1000\,cm^{-1}$ and $E_a = 900\,cm^{-1}$ and (○) $-\Delta E = 4000\,cm^{-1}$ and $E_a = 91\,cm^{-1}$. Note the effects of vibrational mode selectivity at low excess vibrational energies

[51]. For DA charge transfer complexes [53] $\Delta E_{CT} \simeq 12000\,cm^{-1}$. For charge separation we use recent data for barrelene-based DBA supermolecules, which give $\Delta E = 2500 - 6000\,cm^{-1}$ [51].

In Figs. 5 and 6 we present the results of model calculations for the excess vibrational energy dependence of the AFD(E)s for charge recombination and for charge separation. For low and moderate energy gaps ($-\Delta E = 1000 - 4000\,cm^{-1}$), which correspond to charge separation, the AFDs at low values of E reveal an irregular spread (Fig. 6), which reflects mode selectivity. These mode selectivity effects are damped at higher values of E (Fig. 6) and are rather unpronounced for large values of $|\Delta E|$ over the entire E domain (Fig. 5) for charge recombination. For small and moderate values of $|\Delta E|$ the energy dependence of AFD(E) qualitatively changes with increasing $|\Delta E|$ (Fig. 6), reflecting the "transition" from intramolecular normal ET ($-\Delta E < \lambda$) to intramolecular activationless ET ($-\Delta E = \lambda$). These patterns of mode-selective energy dependence of AFD(E) (for small $|\Delta E|$) are of interest for the elucidation of the experimental excess energy dependence of intramolecular ET, explored by Verhoeven et al. in jet-cooled supermolecules [11, 15, 17]. The situation for the energy dependence of AFD(E) for charge recombination (Fig. 5) corresponds to the intramolecular inverted ET which is characterized by (i) AFD(E) (for a fixed ΔE) which decreases with increasing E over the relevant domain, and (ii) AFD($E;\Delta E$) (for a fixed E) which increases with increasing $|\Delta E|$. Feature (ii) reflects the energy gap law for intramolecular ET [16].

This analysis builds a bridge between ET and radiationless transitions in isolated molecules and reflects on the universal unifying features of intramolecular and medium induced nonradiative relaxation.

V. The Dynamics of Ultrahigh Rydbergs

(V.A) Intramolecular Coupling in a Sparse Level Structure

Up to this point we focused on intramolecular chemistry in the isolated molecule statistical limit. Continuing our excursion in the world of intramolecular dynamics, we focus on the sparse level structure (Fig. 2), which manifests the following effects:

(1) A rich spectroscopic level structure in some triatomics, e.g., NO_2, which originates from interstate mixing between a small number of doorway states corresponding to electronically excited vibronic levels and the ground state vibrational manifold.

(2) The Douglas effect [54] of the lengthening of the pure radiative lifetimes of triatomic molecules, e.g., NO_2, SO_2, CS_2 [27]. This effect manifests interstate mixing in a sparse level structure [27, 30–34] with the radiative decay rates $\Gamma^{(j)}_{RAD} = D_j\Gamma$, where Γ is the total radiative width obtained from the integrated oscillator strength. D_j ($\ll 1$) is the dilution factor subjected to the diagonal sum rule $\sum_j D_j = 1$, with the mean value $\langle D_j \rangle \simeq 1/N$,

where N is the number of mixed states. This mixing is alluded to as "dilution".

A modern analogue to the dilution effect, which is induced by external (electric field) perturbations, is manifested in the dynamics of ultrahigh molecular Rydberg states.

(V.B) Molecular Rydbergs and Their Decay Channels

Ultrahigh Rydberg states (characterized by the principal quantum numbers $n = 50-300$) of atoms, molecules and clusters are of considerable interest because of the following reasons:

(1) They constitute one-electron "microsystems", with the mean radius $\langle r\rangle = (3/2)n^2 a_0$ (where a_0 is the Bohr radius), e.g., $\langle r\rangle \simeq 8000$ Å for $n = 100$.
(2) Their investigation allows for the determination of fundamental physical constants [55].
(3) They allow for the study of planetary atoms, i.e., three-body Coulomb systems [56].
(4) Their behavior in external electric and magnetic fields is of interest [57].
(5) They exhibit the effects of long-range Casimir retardation forces, which are manifested on the distance scale $r > 137 a_0$ [58].
(6) They are expected to exhibit huge cross sections $\sigma \sim \pi a_0^2 n^4$ for chemical reactions such as charge exchange [23].
(7) Intramolecular dynamics in a bound level structure, e.g., internal conversions and 'reactive' dynamics, i.e., predissociation and autoionization of high Rydbergs [59–63].

Intramolecular dynamics of high Rydbergs is fascinating. Indeed, in the old days of the development of the theory of intramolecular dynamics it was recognized [59–61] that the nonradiative decay rates of low n ($= 3-5$) Rydbergs of aromatic molecules (as inferred from line broadening) are considerably slower (by $1-2$ orders of magnitude) than that of the intravalence excitations in the same energy domain (see Figs. 7 and 8 for the decay of the $3R_u$ Rydberg of C_6H_6 and C_6D_6, which exhibit a small 20% deuterium isotope effect [63]). The decay channels of low Rydberg states of large molecules below the ionization potential involve both nonreactive internal conversion with a partial width $\Gamma_{IC}(n)$, and reactive predissociation with a partial width $\Gamma_D(n)$. For Rydbergs above the ionization potential (vibrational and/or rotational and/or spin-orbit induced) autoionization channels with a width $\Gamma_A(n)$ open up. Accordingly, the lifetime of a n Rydberg is expected to be

$$\tau(n) = \hbar/\Gamma(n) \ , \tag{12}$$

where the total width is

$$\Gamma(n) = \Gamma_{IC}(n) + \Gamma_D(n) + \Gamma_A(n) \ . \tag{13}$$

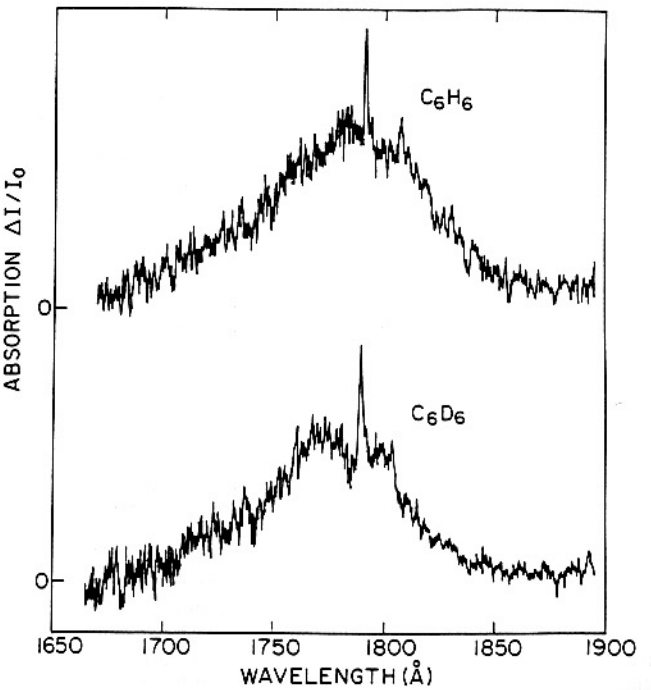

Fig. 7
The absorption spectra of jet-cooled C_6H_6 and C_6D_6 in a linear supersonic expansion of Ar (Amirav and Jortner, Ref. [63]). Note the sharp spectral features, which correspond to the excitation of the electronic origins of the $3R_u$ Rydbergs

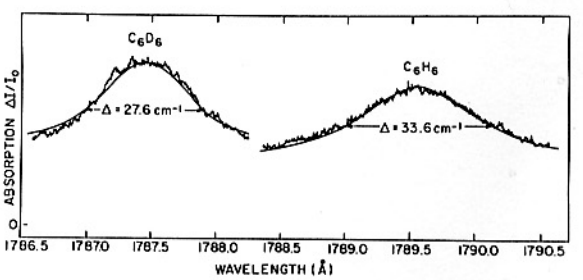

Fig. 8
Lineshape analysis of the $3R_u$ Rydbergs of jet-cooled C_6H_6 and C_6D_6 (Amirav and Jortner, Ref. [63]). The widths (FWHM) of the Lorentzian lineshapes (fitted by the solid lines) correspond to the nonradiative lifetimes of $\tau(C_6H_6) = 154$ fs and $\tau(C_6D_6) = 188$ fs, exhibiting a small (18%) deuterium isotope effect. The decay channels of the $3R_u$ Rydberg correspond to internal conversion and presumably also to predissociation. Note the lack of interference effects between the resonance Rydberg and the broad background $\pi\pi^*$ intravalence absorption, which originates from nearly random coupling effects

Berry's scaling law [64], which was originally developed for autoionization, is expected to hold for all the decay channels, so that the total width of a molecular Rydberg is

$$\Gamma(n) = \Gamma_0/n^3 \ , \tag{14}$$

with the lifetime

$$\tau(n) = (\hbar/\Gamma_0)n^3 \ , \tag{15}$$

where Γ_0 is a numerical constant.

Up to this point we focused on the n dependence of the lifetimes. What about the dependence of the energetics and dynamics on the azimuthal quantum number l? Two characteristics of this l dependence should be noted. Firstly, the lifetimes are l dependent and Eq. (15) has to be modified into the form

$$\tau(n,l) = [\hbar/\Gamma_{0(l)}]n^3 \ , \tag{16}$$

where $\Gamma_{0(l)}$ is an l dependent constant. As intramolecular dynamics is manifested in the spatial region close to the nucleus (range A in Fano's terminology [65, 66]), the short lifetimes are exhibited for low values of l ($=0-3$). When detailed spectroscopic information on a specific molecular Rydberg series is not available, we shall continue to use Eq. (15), with the implicit understanding that $\tau(n)$ and Γ_0 refer to a low value of l. Secondly, the energies of the Rydberg states, which are characterized by the lifetimes (16), are

$$E(n,l) = \mathrm{IP} - \frac{R}{(n-\delta_l)^2} \ , \tag{17}$$

where R is the Rydberg constant, IP is the ionization potential and δ_l is the (l dependent) quantum defect.

(V.C) Long Lifetimes of Ultrahigh Rydbergs

The energetics of ultrahigh molecular Rydbergs ($n = 50-300$) was explored by ZEKE (zero-electron kinetic energy) spectroscopy [67 – 73]. The dynamics of these states (referred to as ZEKE Rydbergs), interrogated by time-resolved ZEKE spectroscopy [19 – 21, 71, 74, 75], provided compelling evidence for the breakdown of Berry's scaling law, Eq. (17), which is manifested by

(1) Long lifetimes of ZEKE Rydbergs of NO. Reiser et al. [69] have observed high lying ($n \gtrsim 100$), very long lived ($\sim \mu$s lifetimes) Rydberg states of NO. Chupka [76, 77] has pointed out that the lifetimes of these states are considerably longer than those expected on the basis of the n^3 scaling law for the predissociative p series of NO.

(2) Dramatic lifetime lengthening of molecular ZEKE Rydbergs. The lifetimes of ZEKE Rydbergs of large molecules are longer by several (2 – 4) orders of magnitude than those expected on the basis of the n^3 scaling relations [19]. The lifetimes of ZEKE Rydbergs ($n = 80-250$) of bis (benzene) chromium (BBC) and 1,4-diaza bicyclo [2,2,2] octane (DABCO) are longer by 2 – 3 orders of magnitude than those expected on the basis of Eqs. (15) and (16) [19].

(V.D) Models

The fascinating novel characteristics of ZEKE Rydbergs triggered extensive theoretical activity, which falls within the framework of two models:

(A) The Rydberg electron-core rotation model [19 – 21, 75]. This model, which implies the dominance of the (classical) dynamics for the Rydberg electron-core rotation coupling, was discussed elsewhere [22].

(B) The (l) or (l, m_l) electric field splitting and mixing model. This model was advanced by Bordas et al. [78], Chupka [76, 77], Merkt and Zare [79], and by us [22], and rests on the following ingredients:

(1) Low l ($=0-3$) states are active in absorption and in intramolecular relaxation.

(2) Stark splitting and mixing of all the l Rydbergs (with a fixed n) is induced by weak stray electric fields ($F \sim 0.01 - 0.1$ V/cm) inevitably present in the system or/and by a weak d.c. background electric field ($F \sim 0.1 - 1$ V/cm) in the experimental ZEKE setup.

(3) A 'democratic' Stark mixing results in the lifetime lengthening for a given manifold, $\tau(n) = (\hbar/\Gamma_0)n^3/D(n)$, where $D(n)$ is the dilution factor. For (l) mixing in a homogeneous electric field [22, 76 – 79] $D(n) \sim 1/n$, while for (l, n_l) mixing induced by a homogeneous electric field, in conjunction with the electric field of ions [79], $D(n) \sim 1/n^2$. For $n = 100$, lengthening of the lifetimes by a huge numerical factor of $10^2 - 10^4$ is expected.

(V.E) The Dilution

The Stark mixing is formally analogous to intramolecular coupling (Fig. 9). The nature and the details of the couplings are qualitatively different. For intramolecular (interstate and intrastate) coupling the doorway state couples in parallel to the entire background manifold and the individual relevant coupling terms are of comparable magnitude. On the other hand, for the electric field-induced coupling between the zero-order Rydbergs, the coupling is [80] (i) sequential, with $l-(l\pm1)$ nonvanishing matrix elements, and (ii) hierarchical, with the sequential matrix elements decreasing with increasing l, being proportional to n^2 for low l and being proportional to n for high l. This qualitative difference between intramolecular and Rydberg coupling also results in a difference in the mixed level structure. For intramolecular coupling the doorway state is usually located within the energy domain of the background manifold and mixed with it. On the other hand, when field-

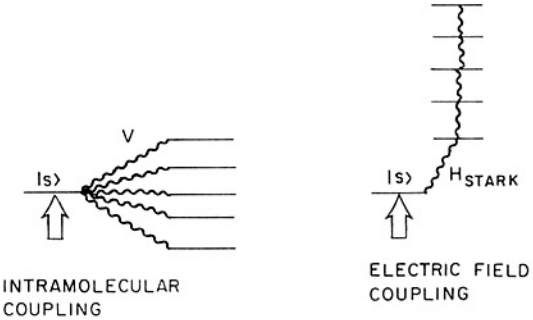

Fig. 9
An artist's view of the analogy between interstate coupling in the sparse limit and field-induced Stark coupling of a Rydberg manifold

induced mixing of Rydbergs with increasing F is accomplished at a constant n, the doorway state does not energetically overlap the Stark split inactive manifold, but rather approaches it from its low energy range (Fig. 10). This problem is analogous to the coupling of a discrete zero-order state with a manifold, which is bound from below [81].

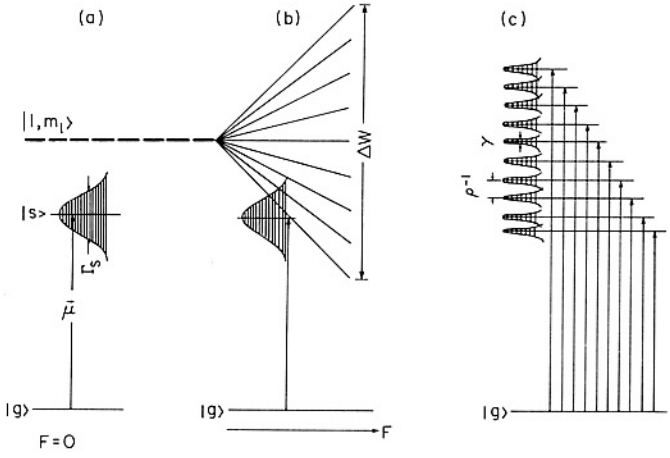

Fig. 10
A schematic energy level scene for the splitting and mixing of Rydberg states in an external electric field. (a) $F = 0$. The low l doorway state $|s\rangle$ is separated from the high l degenerate manifold. The $|s\rangle$ state carries an oscillator strength from the ground state (denoted by a vertical arrow) and has a total nonradiative decay width Γ_s, which constitutes a sum of the partial decay widths of all, e.g., internal conversion, predissociation, and/or autoionization, channels. (b) The F dependence of the splitting of the high l manifold in the external field, which results in the onset of the merging of the $|s\rangle$ state into the manifold. (c) Mixed independently decaying levels at a finite field. All these levels carry oscillator strengths from the ground state

We can now use the arsenal of intramolecular dynamics for the Stark (l) coupling and dynamics (Fig. 10). (a) The relevant discrete level structure consists of a low l state(s) and a hydrogenic manifold of high l. (b) The few low l state(s) constitute the doorway state(s) for excitation. (c) The low l state(s) are coupled to decay channels, i.e., internal conversion, predissociation and/or autoionization. For the sake of simplicity we shall represent the doorway state(s) $|s\rangle$ by a single state (characterized by a low value(s) of $l = l_s$ and $m = m_s$) with the energy $E_s = \mathrm{IP} - R/(n-\delta)^2$ and the total nonradiative decay width $\Gamma_s = \Gamma_0/n^3$. At zero field this state is separated from the degenerate hydrogenic manifold of (n^2-1) high l, m_l states ($l > l_s$) with the energies $E_l = \mathrm{IP} - R/n^2$ and decay widths $\Gamma_l = 0$, which are not optically accessible from the ground state (Fig. 10). In the presence of a weak homogeneous electric field F, the Rydberg level structure and dynamics are determined by the effective Hamiltonian (see Eqs. (1) and (2) of Sect. II) for this system

$$\boldsymbol{H}_{\mathrm{eff}} = \boldsymbol{H}_0 + \boldsymbol{H}_{\mathrm{STARK}} - (\mathrm{i}/2)\boldsymbol{\Gamma} \ , \tag{18}$$

where $\boldsymbol{H}_0$ is the (diagonal) field-free Hamiltonian with the energies E_s and $\{E_l\}$. $\boldsymbol{\Gamma}$ is the decay matrix with the elements Γ_s, $\{\Gamma_l = 0\}$. $\boldsymbol{H}_{\mathrm{STARK}}$ is the Stark Hamiltonian with the operator eFz coupling the doorway state $l_s m_s$ and the states $\{l', m'\}$ with $l' = l_s + 1$, $m' = m_s$, while the states $\{l, m_l\}$ are coupled with $\{l' = l \pm 1, m_l\}$. The $n \times n$ effective Hamiltonian (18) for $m = m_s = 0$ can be diagonalized by a complex orthogonal transformation, resulting in the independently decaying levels of the system

$$|j\rangle = a_s^{(j)}|s\rangle + \sum_l b_l^{(j)}|l, m_s\rangle \ , \tag{19}$$

where $a_s^{(j)}$ and $\{b_l^{(j)}\}$ are (complex) coefficients. The (complex) eigenvalues are $[E_j - (\mathrm{i}/2)\gamma_j]$, where E_j are the energy levels and γ_j the decay rates of the molecular eigenstates. (From now on we shall set $\hbar = 1$ in all our equations.) The input parameters required for the diagonalization of the effective Hamiltonian (at constant F) are the quantum defect δ (mod 1) extracted from Rydberg energetics, and the width parameter Γ_0 extracted from low Rydberg line broadening, which are obtained from experimental data.

(V.F) Strong Mixing

When the energetic spread of the Stark manifold

$$\Delta W = 6Rn^2(F/5.15 \times 10^9) \tag{20}$$

(where F is expressed in V/cm) exceeds the zero-field splitting $2\delta R/n^3$ of the doorway state, i.e., $2\delta R/n^3 < \Delta W/2$, the strong mixing of the $|s\rangle$ state with the $\{|l, m_l\rangle\}$ manifold will be realized. The onset of the strong mixing at a fixed n occurs for an electric field

$$F > 3.4 \times 10^5 \delta/n^5 \ , \tag{21}$$

or, alternatively, the lower limit for the n value where strong mixing prevails is $n_M = 80.5\,\delta^{1/5}(F/\mathrm{Vcm}^{-1})^{-1/5}$. For typical long Rydberg series of large molecules [19], Even et al. found $\delta = 0.41$ for DABCO and $\delta = 1.38$ (δ (mod 1) = 0.38) for BBC, so that for both of these molecular Rydbergs $n_{\mathrm{M}} \simeq 67\,(F/\mathrm{Vcm}^{-1})^{-1/5}$. In the strong mixing limit for (l) mixing, for $n \geq n_{\mathrm{M}}$ the average lifetime of the diluted states is $\gamma^{-1} \simeq n\tau_s$, where $\tau_s = \hbar/\Gamma_s = \hbar n^3/\Gamma_0$ is the lifetime of the $|s\rangle$ state.

(V.G) The Rise and Fall of the Mixed Rydberg Level Structure

We shall be concerned with the optical excitation to and the decay of the mixed level structure, Eq. (19), of a single high n (or several high n) manifold(s) subjected to l mixing. To make contact with real life situations we consider two experimental observables [22]:

(a) The excited-state total population probability $P(t)$. This corresponds to the time-dependent population of the entire Rydberg manifold. $P(t)$ is interrogated by time-resolved ZEKE spectroscopy, by the application of the extracting pulsed electric field at the decay time t after the laser field. For a broad band excitation of a sparse

mixed level structure, when $\Delta\omega_p \gg \Delta W$, where $\Delta\omega_p$ is the spectral width of the laser pulse, and ΔW is the energetic spread of the Rydberg manifold, Eq. (20), the population probability is [22]

$$P(t) = \sum_j |a_s^{(j)}|^2 \exp(-\gamma_j t) \ , \tag{22}$$

exhibiting a superposition of exponentials at all times t. We note that no interference effects (i.e., quantum beats) in the decay are exhibited for $P(t)$.

(b) The population probability $I(t)$ of the doorway state $|s\rangle$. $I(t)$ represents the time-dependent population of the low angular momentum state(s) $|s\rangle$, which is (are) active in absorption. In principle, $I(t)$ could be monitored by time-resolved fluorescence to the ground state, however, the extremely low oscillator strengths (and extremely long radiative lifetimes, i.e., $\propto n^3$) of high Rydbergs preclude this approach. $I(t)$ can be experimentally interrogated by the subsequent photoionization of the Rydberg manifold, with the doorway state being also the active state for ionization. For a broad band excitation [22]

$$I(t) = \sum_j |a_s^{(j)}|^4 \exp(-\gamma_j t) + \sum_j \sum_{j'} |a_s^{(j)}|^2 |a_s^{(j')}|^2 \times \exp[i(E_j - E_{j'})] \exp[-(\gamma_j + \gamma_{j'})t/2] \ , \tag{23}$$

consisting of direct decay terms and of oscillatory interference terms. The latter exhibit quantum beats, i.e., temporal coherence effects.

All the available experimental information on the dynamics of ultrahigh Rydbergs emerges from time-resolved ZEKE experiments. These experiments are performed using conventional ns lasers with $\Delta\omega_p = 0.1 - 0.5\ \mathrm{cm}^{-1}$. To characterize the experimental conditions we take for Eq. (20) $\Delta W = 1.3 \times 10^{-4}\, n^2\, (F/\mathrm{Vcm}^{-1})$, and obtain $\Delta W = 0.13\ \mathrm{cm}^{-1}$ for $n = 100$ at $F = 0.1$ V/cm. Accordingly, $\Delta\omega_p > \Delta W$, whereupon the broad band excitation will be accomplished under ns excitation. The population decay $P(t)$ is expected to be given by Eq. (22). The decay will not be strictly exponential, reflecting the distribution of the decay lifetimes for a fixed external field.

(V.H) Field-Induced Mixing Within a Single Rydberg Manifold

To explore the general features of field-induced (l) mixing, we consider the dilution within the high Rydbergs of the DABCO molecule, which was studied by Even et al. [19]. The $n = 10-30$ Rydbergs of DABCO [19] exhibit three series. The prominent Rydberg series, with the largest quantum defect, is tentatively assigned to the s ($l = 0$) series [19]. This prominent Rydberg series is characterized by the parameters [19]

$$\delta = 0.41$$
$$\Gamma_0 = 3 \times 10^3\ \mathrm{cm}^{-1} \tag{24}$$

for the quantum defect and the decay widths, respectively. We shall take a single doorway state for each n, which is characterized by the parameters (24). This single doorway state, taken as $|s\rangle = |l = 0, m_l = 0\rangle$ is mixed by hierarchical and sequential Stark coupling with the inactive manifold $\{|l, m_l = 0\rangle\}$. It will be also useful to specify the homogeneous electric field in terms of reduced units, i.e.,

$$\bar{F} = (F/\mathrm{Vcm}^{-1}) n^5 / 3.4 \times 10^9 \delta \ . \tag{25}$$

For $\bar{F} = 0$ the isolated $|s\rangle$ resonance is characterized by the lifetime

$$\tau_s = \hbar/\Gamma_s = \hbar n^3/\Gamma_0 \ . \tag{26}$$

The diagonalization of the effective Hamiltonian, Eq. (18), for fixed values of n, δ, Γ_s and F results in the following

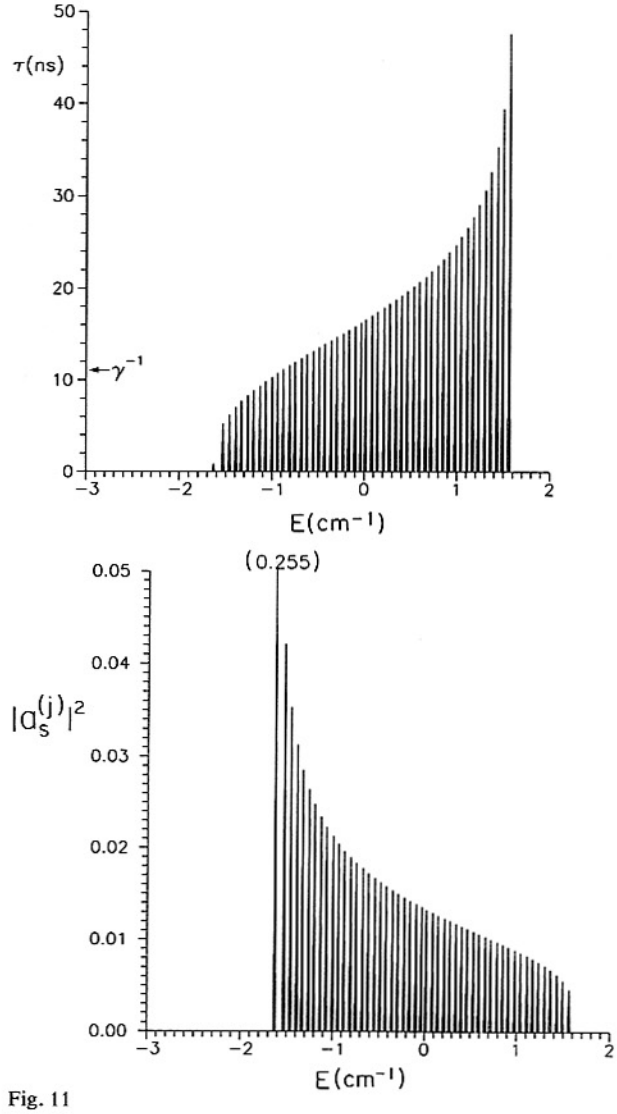

Fig. 11
The lifetime and accessibility spectra for $n = 50$ Rydberg manifold of DABCO for $F = 10$ V/cm ($\bar{F} \equiv 2.1$). (a) The lifetime spectrum (τ_j vs. E_j). Note the lowest energy shortest lifetime $\tau_1 = 0.3$ ns. The average-diluted lifetime $\gamma^{-1} = n\tau_s = 11$ ns is marked by an arrow. (b) The accessibility spectrum ($|a_s^{(j)}|^2$ vs. E_j). The amplitude of the doorway state in the lowest energy, shortest lifetime state is $|a_s^{(1)}|^2 = 0.255$

relevant parameters: (i) the energies E_j, (ii) the lifetimes $\tau_j = \hbar/\gamma_j$ and (iii) the mixing coefficients of the doorway state $|a_s^{(j)}|^2$.

Model calculations were performed for $n = 50$ and $n = 100$ manifolds of DABCO. In Fig. 11 we present the lifetime spectra (τ vs. E) and the accessibility spectra ($|a_s^{(j)}|^2$ vs. E) for $n = 50$ at $F = 10$ V/cm ($\bar{F} = 2.1$), while a typical lifetime-accessibility map for $n = 50$ at $F = 20$ V/cm ($\bar{F} = 4.5$) is portrayed in Fig. 12. The lowest energy, short lifetime (Fig. 11a) of $\tau_1 = 0.3$ ns, is close to the value of $\tau_s = 0.22$ ns, Eq. (26), with a weight (Fig. 11b) of $|a_s^{(1)}|^2 = 0.26$. This short lifetime corresponds to the residue of the doorway state. The distribution of the longer lifetimes (Figs. 11a and 12) represents the diluted states. The lifetimes and amplitudes spectra are asymmetric, with τ_j increasing at higher energies (Fig. 11a), while $|a_s^{(j)}|^2$ decrease with increasing energy (Fig. 11b). Consequently, the lifetime accessibility spectrum is also asymmetric with longer lifetimes being characterized by smaller amplitudes (Fig. 12). These features manifest the effects of the sequential Stark coupling. The average value of $\gamma^{-1} = n\tau_s = 11$ ns falls in the middle of the asymmetric distribution.

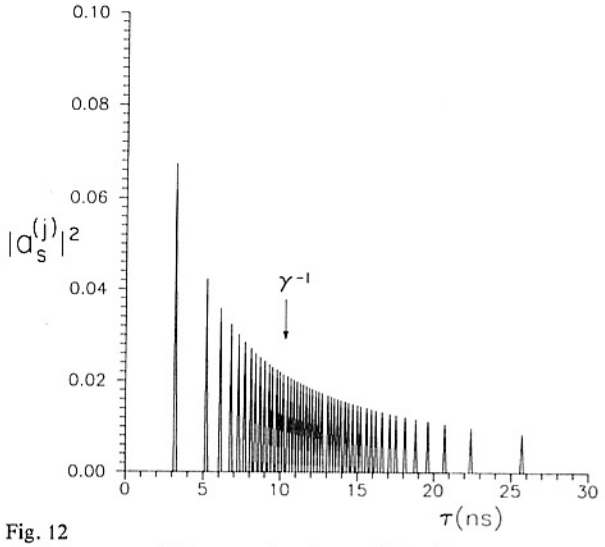

Fig. 12
A lifetime-accessibility map for the $n = 50$ Rydberg manifold of DABCO for $F = 20$ V/cm ($\bar{F} = 4.4$). The average-diluted lifetime $\gamma^{-1} = n\tau_s = 11$ ns is marked by an arrow

(V.I) The Hierarchy of the Two Time Scales

To provide a physical picture of the evolution of the field-induced mixing with increasing F, we present in Fig. 13 the lifetime-accessibility maps (plotted as $|a_s^{(j)}|^2$ vs. the decay widths γ_j) of $n = 100$ for $F = 0.1$ V/cm ($\bar{F} = 0.72$), 0.2 V/cm ($\bar{F} = 1.44$) and 0.3 V/cm ($\bar{F} = 2.2$). These $\bar{F}$ values span the range from weak coupling towards strong coupling. The lifetime of the doorway state is $\tau_s = 1.8$ ns. These results exhibit the following features:

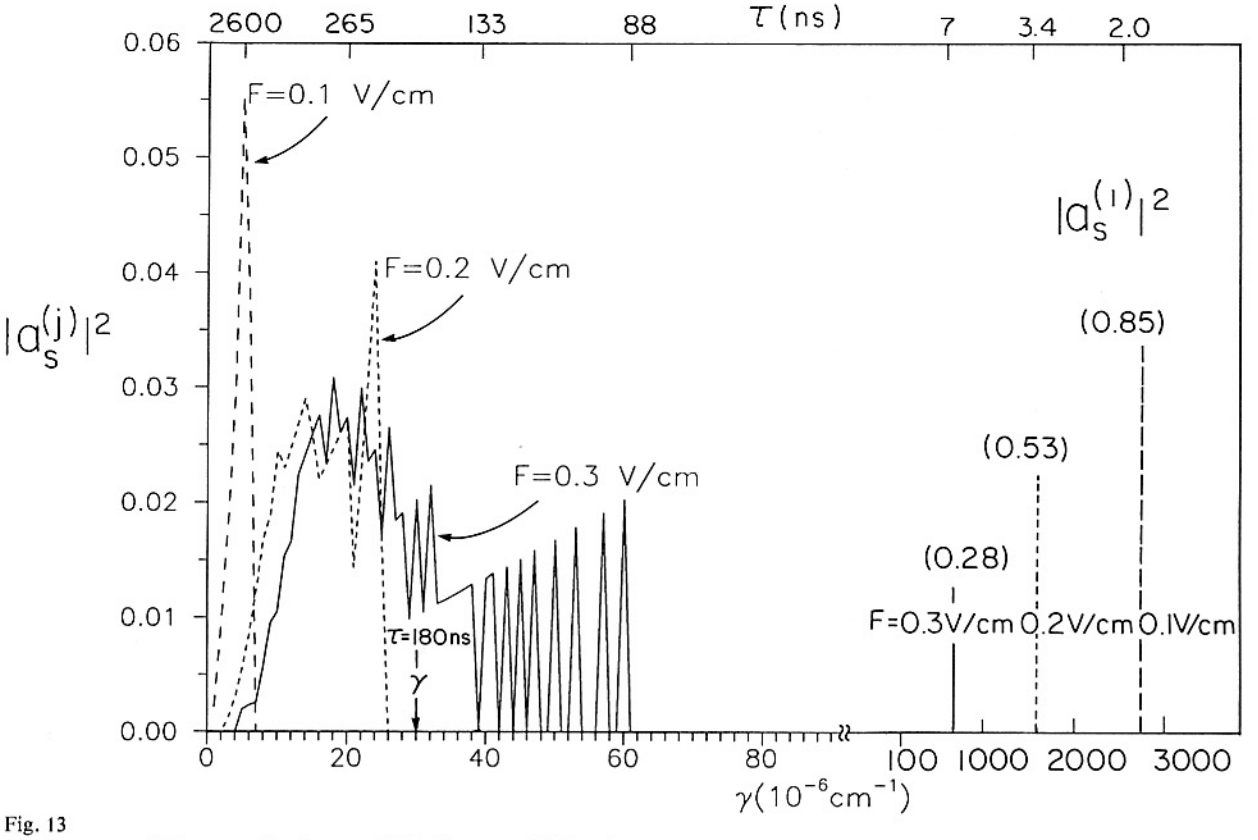

Fig. 13
Lifetime-accessibility maps for the $n = 100$ Rydberg manifolds of DABCO for $F = 0.1$, 0.2 and 0.3 V/cm. Note the two distinct time scales. The short lifetimes are specified by the amplitudes $|a_s^{(1)}|^2$ (in brackets). The long lifetimes exhibit a broad distribution. The average-diluted lifetime $\tau = n\tau_s = 180$ ns (marked by an arrow) provides a reasonable mean value for the distribution at $F = 0.3$ V/cm ($\bar{F} = 2.2$)

(1) Two distinct time scales for the decay are exhibited.
(2) A short lifetime τ_{SHORT} appears in the range of $\tau_{SHORT} = 2.0 - 7.0$ ns. These short decay times represent the residues of the doorway state, as is evident from the decrease of their amplitude $|a_s^{(1)}|^2$ with increasing $\bar{F}$ (Fig. 13). τ_{SHORT} for low $\bar{F}$ is close to τ_s, while with increasing $\bar{F}$, τ_{SHORT} becomes longer.
(3) A broad distribution of long decay times $\{\tau_{LONG}\}$. This distribution of the lifetimes corresponds to the diluted states, which have parentage in the inactive $l \neq 0$ manifold. For weak mixing ($\bar{F} = 0.72$) the distribution of these long lifetimes is rather narrow with a maximum in the μs time range. With increasing $\bar{F}$ this distribution becomes broader. At $\bar{F} = 2.2$, which approaches the strong mixing limit, a broad distribution around the mean value of $\gamma^{-1} = n\tau_s = 180$ ns is exhibited.

For the sake of the critical reader we present in Fig. 14 the time evolution of the total population $P(t)$, Eq. (22). $P(t)$ exhibits a bimodal population decay, which is distinct from dephasing, being characterized by the two time scales:

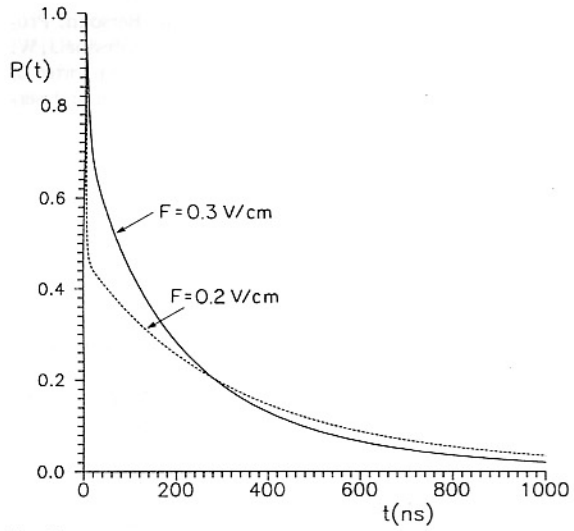

Fig. 14
The time-resolved total population of the $n = 100$ manifold of DABCO at $F = 0.2$ V/cm and at $F = 0.3$ V/cm

Range (I): The short lifetime τ_{SHORT}.
Range (II): The distribution of long lifetimes $\{\tau_{LONG}\}$ with the average value $\langle\tau_{LONG}\rangle$.

To provide a reasonable approximate description of the electric field dependence of the decay lifetimes, we consider their dependence on the weight $|a_s^{(1)}|^2$ of the lower energy eigenstates, i.e., the residue of the doorway state. In Fig. 15 we present the electric field dependence of the short lifetime τ_{SHORT} and of the averaged value of the long lifetime $\langle\tau_{LONG}\rangle$. τ_{SHORT} is well represented by

$$\tau_{SHORT} \simeq \tau_s / |a_s^{(1)}|^2 \ . \tag{27}$$

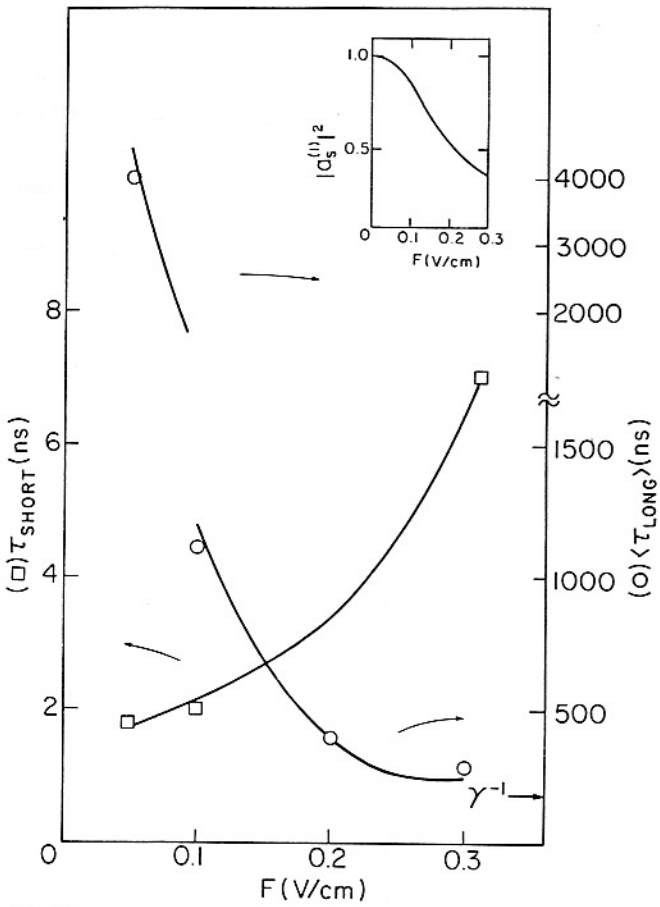

Fig. 15
The electric field dependence of the short lifetime τ_{SHORT} and of the average long lifetime $\langle\tau_{LONG}\rangle$ for the $n = 100$ manifold of DABCO. The insert shows the electric field dependence of the weight $|a_s^{(1)}|^2$ of the doorway state within the lowest energy eigenstate. The solid lines represent the description of τ_{SHORT} by Eq. (27) and of $\langle\tau_{LONG}\rangle$ by Eq. (28)

For a broad distribution of the long lifetimes a crude approximation for the mean value is

$$\langle\tau_{LONG}\rangle \simeq n\tau_s/(1 - |a_s^{(1)}|^2) \ . \tag{28}$$

As is evident from Fig. 15, Eqs. (27) and (28) provide a good description of the time scales of decay times.

The total population probability in the weak mixing regime is approximately given by the superposition of the contributions from the two time domains, in the form

$$P(t) \simeq |a_s^{(1)}|^2 \exp(-t/\tau_{SHORT}) + (1 - |a_s^{(1)}|^2) \exp(-t/\langle\tau_{LONG}\rangle) \ . \tag{29}$$

With the increase of $\bar{F}$ above $\bar{F} > 1$ we expect that, in range (I), τ_{SHORT} increases (towards $n\tau_s$) and the amplitude $|a_s^{(1)}|^2$ of the short component decreases, while in range (II) the average diluted value of $\langle\tau_{LONG}\rangle$ tends towards $n\tau_s$. The strong mixing limit is realized for $\bar{F} > 1$ with $|a_s^{(1)}|^2 \to 1/n$, τ_{SHORT}, $\langle\tau_{LONG}\rangle \to n\tau_s$. Then contribu-

tion of range (I) to $P(t)$, Eq. (29), becomes small and indistinguishable from that of range (II), which provides the dominating contribution to $P(t)$ with the mean lifetime $\tau_s/D(n)$. This heuristic, but physical, description predicts that:

(1) Two distinct ($\sim$ ns and $\sim$ μs) time scales for the dynamics for $\bar{F}<1$ will be exhibited.
(2) The lengthening of the short (ns) temporal decay component with increasing $\bar{F}$ is expected for $\bar{F}<1$.
(3) A broad distribution of long lifetimes with the average value of $\simeq(10-20)n\tau_s$, i.e., in the μs time domain, is expected for $\bar{F}<1$.
(4) The long lifetimes exhibit a broad distribution.
(5) The average long lifetime decreases with increasing $\bar{F}$.
(6) Coalescence of the lifetimes towards the mean diluted lifetime $n\tau_s$ occurs in the strong mixing limit ($\bar{F}>1$).

These predictions for the novel and rich dynamics in the weak mixing ($\bar{F}<1$) domain provide guidelines for the understanding of experimental data. In particular, our analysis provides clues for:

(a) The possibility of observation of extremely long ($\sim$ a few μs) lifetimes of ZEKE Rydbergs [69–72].
(b) Pronounced non-exponentiality of the long-time decay of ZEKE Rydbergs [19, 20].
(c) The dramatic (two to three orders of magnitude) break in the Rydberg lifetimes vs. n [19] corresponds to the 'transition' from range (I) to range (II), which occurs at $n\simeq n_M$ ($\bar{F}\sim 1$), when the contribution of range (II) to the decay dynamics becomes dominant.

The central prediction for the occurrence of two distinct time scales for the dynamics of Rydbergs ($\bar{F}<1$) was not yet verified experimentally. Our analysis calls for the extension of the time-resolved ZEKE technique into the time domain of 1–10 ns.

(V.J) Summing-Up

We have provided a physical picture for the dynamics of ultrahigh Rydbergs in an external (homogeneous) electric field, which bears a close analogy to intramolecular dynamics. From the technical point of view the picture of the dynamics of ultrahigh Rydbergs has to be, and was [82], extended to include the following effects:

(1) Mixing of several n manifolds. When $\bar{F}<1/\delta$ the mixing between neighboring n manifolds is negligible, whereupon our treatment of a single $n=100$ manifold in the preceding section (V.I) is valid. When $\bar{F}>1/\delta$, the mixing of several doorway states, e.g., $|n,l=0\rangle$ of different n with the corresponding inactive, e.g., $\{|n,l\neq 0\rangle\}$, manifolds of distinct n values, will be significant. The level structure and the accessibility-lifetime maps are qualitatively modified. Our model calculations [82] for the mixing of five n manifolds ($n=48-52$) with the parameters given by Eq. (28), show that in the strong mixing limit ($\bar{F}\gg 1$) the overall features of the decay are similar to that of the single n manifold.
(2) Multichannel mixing. In the simple picture, which rests on a single l (e.g., $l=0$), the doorway state with a decay width Γ_0/n^3, has to be extended. Several low l states ($l=0-3$), each characterized by a distinct quantum defect δ_l and a decay width $\Gamma_0(l)/n^3$, have to be incorporated in the effective Hamiltonian, Eq. (18). In some cases, when several of these low l states decay to a common channel, the decay matrix $i\Gamma/2$ in Eq. (18) is non-diagonal. The accessibility of the doorway state(s) is determined by the specific, e.g., one-photon or two-photon excitation conditions. Multichannel coupling quantitatively modifies the level mixing and the effect of the external weak electric field on the time-resolved decay, as we have found for the dynamics of the Rydbergs of NO [82].

From the point of view of general methodology we have focused on the dynamics of ultrahigh mixed Rydberg manifolds. Our analysis provides a universality principle for a unified description of the level structure and dynamics of high Rydbergs of molecules and of autoionizing atoms.

We are grateful to Professor U. Even, Professor R. Bersohn, Professor O. Cheshnovsky, Professor R.D. Levine, and Professor J.W. Verhoeven, for stimulating discussions. This research was supported in part by the German-Israel Binational James Franck Program on laser-matter interactions.

References

[1] G.L. Closs, L.T. Calcaterra, N.J. Green, K.W. Penfield, and J.R. Miller, J. Phys. Chem. *90*, 3673 (1986).
[2] C.A. Stein, N.A. Lewis, and G.J. Seitz, J. Am. Chem. Soc. *104*, 2596 (1982).
[3] S.S. Isied, W. Vassilian, J.F. Wishart, C. Creutz, H.A. Schwarz, and N. Sutin, J. Am. Chem. Soc. *109*, 635 (1988).
[4] K.W. Penfield, J.R. Miller, M.N. Paddon-Row, E. Cotsaris, A.M. Oliver, and N.S. High, J. Am. Chem. Soc. *109*, 5061 (1987).
[5] J. Jortner and M. Bixon, Mol. Cryst. Liq. Cryst. *234*, 29 (1993).
[6] R.A. Marcus, J. Chem. Phys. *966*, 979 (1956).
[7] R.A. Marcus, Ann. Rev. Phys. Chem. *15*, 155 (1964).
[8] M.D. Newton and N. Sutin, Ann. Rev. Phys. Chem. *35*, 437 (1984).
[9] R.A. Marcus and N. Sutin, Biochim. Biophys. Acta *811*, 265 (1985).
[10] J. Jortner, M. Bixon, H. Heitele, and M.E. Michel-Beyerle, Chem. Phys. Lett. *197*, 131 (1992).
[11] J. Jortner, M. Bixon, B. Wegewijs, J.W. Verhoeven, and R.P.H. Rettschnick, Chem. Phys. Lett. *205*, 451 (1993).
[12] M. Bixon and J. Jortner, J. Phys. Chem. *97*, 13061 (1993).
[13] B. Wegewijs, R.M. Hermant, J.W. Verhoeven, A.G.M. Kunst, and R.P.H. Rettschnick, Chem. Phys. Lett. *140*, 587 (1987).
[14] R.M. Hermant, B. Wegewijs, J.W. Verhoeven, A.G.M. Kunst, and R.P.H. Rettschnick: Recl. Trav. Chim. Pays-Bas *107*, 349 (1988).
[15] B. Wegewijs, A.K.F. Ng, R.P.H. Rettschnick, and J.W. Verhoeven: Chem. Phys. Lett. *200*, 357 (1992).
[16] J. Jortner and M. Bixon, J. Photochem. Photobiol. *A82*, 5 (1994).
[17] J.W. Verhoeven, B. Wegewijs, J. Kroon, R.P.H. Rettschnick, M.N. Paddon-Row, and A.M. Oliver, J. Photochem. Photobiol. A*82*, 161 (1994).

[18] Edited by J. Jortner and B. Pullman, Perspectives in Photosynthesis, Dordrecht, Kluwer 1990.
[19] U. Even, R.D. Levine, and R. Bersohn, J. Phys. Chem. *98*, 3472 (1994).
[20] D. Bahatt, U. Even, and R.D. Levine, J. Chem. Phys. *98*, 1744 (1993).
[21] U. Even, M. Ben-Nun, and R.D. Levine, Chem. Phys. Lett. *210*, 416 (1993).
[22] J. Jortner and M. Bixon, J. Chem. Phys. (submitted).
[23] J. Wang and R.E. Olson, Phys. Rev. Lett. *72*, 332 (1994).
[24] M. Bixon and J. Jortner, J. Chem. Phys. *48*, 715 (1968).
[25] M. Bixon and J. Jortner, Mol. Cryst. *213*, 237 (1969).
[26] M. Bixon and J. Jortner, Isr. J. Chem. *1*, 189 (1969).
[27] M. Bixon and J. Jortner, J. Chem. Phys. *50*, 3284 (1969).
[28] M. Bixon and J. Jortner, J. Chem. Phys. *50*, 4061 (1969).
[29] M. Bixon, Y. Dothan, and J. Jortner, Mol. Phys. *17*, 109 (1969).
[30] S. Mukamel and J. Jortner, in: The World of Quantum Chemistry. Ed. by R. Daudel and B. Pullman, Proc. First Intl. Congress Quantum Chemistry, pp. 145–209, Menton, France 1973, D. Reidel Publ. Co. 1974.
[31] S. Mukamel and J. Jortner, in: MTP International Review of Science, Vol. 13, p. 327. Ed. by A.D. Buckingham and C.A. Coulson, Butterworth, London 1976.
[32] S. Mukamel and J. Jortner, in: Excited States, Vol. III, pp. 57–107. Ed. by E.C. Lim, Academic Press 1977.
[33] J. Kommandeur and J. Jortner, Chem. Phys. *28*, 273 (1978).
[34] R.D. Levine and J. Jortner, in: Advances in Chemical Physics, Vol. 47, pp. 1–114. Ed. by J. Jortner, R.D. Levine, and S.A. Rice, Wiley, New York 1981.
[35] K. Huang and A. Rhys, Proc. R. Soc. *A208*, 352 (1951).
[36] R. Kubo, Phys. Rev. *86*, 929 (1952).
[37] M. Lax, J. Chem. Phys. *20*, 1752 (1952).
[38] R. Kubo and Y. Toyozawa, Prog. Theor. Phys. *13*, 160 (1955).
[39] Th. Förster, Discuss. Faraday Soc. *27*, 7 (1959).
[40] M. Kasha, Rad. Res. Suppl. *2*, 243 (1960).
[41] M. Beer and H.C. Longuet Higgins, J. Chem. Phys. *23*, 1390 (1955).
[42] G.W. Robinson and R.P. Frosch, J. Chem. Phys. *37*, 1962 (1962).
[43] M. Gouterman, J. Chem. Phys. *36*, 2846 (1962).
[44] S.H. Lin, J. Chem. Phys. *44*, 3759 (1966).
[45] S.H. Lin and R. Bersohn, J. Chem. Phys. *48*, 2732 (1968).
[46] G.B. Kistiakowski and C.S. Parmenter, J. Chem. Phys. *42*, 2942 (1965).
[47] A. Amirav and J. Jortner, J. Chem. Phys. *81*, 4200 (1984).
[48] A. Amirav, M. Sonnenschein, and J. Jortner, J. Phys. Chem. *88*, 5593 (1984).
[49] U. Even and J. Jortner, J. Chem. Phys. *77*, 4391 (1982).
[50] A. Amirav, H. Horowitz, and J. Jortner, J. Chem. Phys. *88*, 3092 (1988).
[51] J. Cortes, H. Heitele, and J. Jortner, J. Phys. Chem. *98*, 2527 (1994).
[52] R.D. Russel and D.H. Levy, J. Phys. Chem. *86*, 2718 (1982).
[53] F. Markel, N.S. Rerris, I.R. Gould, and A.B. Myers, J. Am. Chem. Soc. *114*, 6208 (1992).
[54] A.E. Douglas, J. Chem. Phys. *45*, 1007 (1966).
[55] J. Liang, M. Gross, P. Goy, and S. Haroche, Phys. Rev. *A33*, 4437 (1986).
[56] J. Müller and J. Burgdörfer, Phys. Rev. Lett. *70*, 2375 (1993).
[57] Edited by R.F. Stebbing and F.B. Dunning, Rydberg States of Atoms and Molecules, University Press, Cambridge, New York 1983.
[58] Edited by F.S. Levin and D.A. Micha, Long Range Casimir Forces, Plenum Press, New York 1993.
[59] J. Jortner, J. Chim. Phys. Special Issue, Transitions Non Radiatives Dans Les Molécules (1969).
[60] J. Jortner and S. Leach, J. Chim. Phys. *77*, 7 (1980); J. Jortner and S. Leach, J. Chim. Phys. *77*, 43 (1980).
[61] J. Jortner and G.C. Morris, J. Chem. Phys. *51*, 3689 (1969).
[62] R.L. Whetten, S.G. Grubb, C.E. Otis, A.C. Albrecht, and E.R. Grant, J. Chem. Phys. *82*, 1115 (1985).
[63] A. Amirav and J. Jortner, J. Chem. Phys. *82*, 4378 (1985).
[64] R.S. Berry, J. Chem. Phys. *45*, 1228 (1966).
[65] U. Fano, Phys. Rev. *A2*, 353 (1970).
[66] U. Fano, J. Opt. Soc. Am. *65*, 979 (1975).
[67] K. Müller-Dethlefs, M. Sander, and E.W. Schlag, Chem. Phys. Lett. *112*, 291 (1984).
[68] K. Müller-Dethlefs, M. Sander, and E.W. Schlag, Z. Naturforsch. *38A*, 1089 (1984).
[69] G. Reiser, W. Habenicht, K. Müller-Dethlefs, and E.W. Schlag, Chem. Phys. Lett. *152*, 119 (1988).
[70] K. Müller-Dethlefs and E.W. Schlag, Ann. Rev. Phys. Chem. *42*, 109 (1991).
[71] W.G. Scherzer, H.L. Selzle, E.W. Schlag, and R.D. Levine, Phys. Rev. Lett. *72*, 1435 (1994).
[72] W.G. Scherzer, H.L. Selzle, and E.W. Schlag, Z. Naturforsch. *48A*, 1256 (1993).
[73] F. Merkt and T.P. Softley, Int. Rev. Phys. Chem. *12*, 205 (1993).
[74] F. Merkt, J. Chem. Phys. *100*, 2623 (1994).
[75] E. Rabani, L.Ya. Baranov, R.D. Levine, and U. Even, Chem. Phys. Lett. *221*, 473 (1994).
[76] W.A. Chupka, J. Chem. Phys. *98*, 4520 (1993).
[77] W.A. Chupka, J. Chem. Phys. *99*, 5800 (1993).
[78] C. Bordas, P.F. Brevet, M. Broyer, J. Chevaleyre, P. Labastie, and J.P. Perrot, Phys. Rev. Lett. *60*, 917 (1988).
[79] F. Merkt and R.N. Zare, J. Chem. Phys. *101*, 3495 (1994).
[80] H.A. Bethe and E.E. Salpeter, Quantum Mechanics of One- and Two-Electron Atoms, Springer Verlag, Berlin 1957.
[81] M. Gelbart and J. Jortner, J. Chem. Phys. *54*, 2070 (1971).
[82] M. Bixon and J. Jortner (to be published).

Presented at the Discussion Meeting of the Deutsche Bunsen-Gesellschaft für Physikalische Chemie "Molecular Spectroscopy and Molecular Dynamics: Theory and Experiment" in Grainau, August 28th to September 1st, 1994

E 8865